Faster Form of Electron Magnetic Reconnection with a Finite Length X-Line

P. S. Pyakurel[1,*] M. A. Shay,[2] J. F. Drake,[3] T. D. Phan,[1] P. A. Cassak,[4] and J. L. Verniero[1]

[1]*Space Sciences Laboratory, University of California, Berkeley, California 94720, USA*
[2]*University of Delaware, Newark, Delaware 19716, USA*
[3]*Department of Physics and the Institute for Physical Science and Technology, University of Maryland,*
College Park, Maryland 20742, USA
[4]*Department of Physics and Astronomy and Center for KINETIC Plasma Physics, West Virginia University,*
Morgantown, West Virginia 26506, USA

Observations in Earth's turbulent magnetosheath downstream of a quasiparallel bow shock reveal a prevalence of electron-scale current sheets favorable for electron-only reconnection where ions are not coupled to the reconnecting magnetic fields. In small-scale turbulence, magnetic structures associated with intense current sheets are limited in all dimensions. And since the coupling of ions are constrained by a minimum length scale, the dynamics of electron reconnection is likely to be 3D. Here, both 2D and 3D kinetic particle-in-cell simulations are used to investigate electron-only reconnection, focusing on the reconnection rate and associated electron flows. A new form of 3D electron-only reconnection spontaneously develops where the magnetic X-line is localized in the out-of-plane (z) direction. The consequence is an enhancement of the reconnection rate compared with two dimensions, which results from differential mass flux out of the diffusion region along z, enabling a faster inflow velocity and thus a larger reconnection rate. This outflow along z is due to the magnetic tension force in z just as the conventional exhaust tension force, allowing particles to leave the diffusion region efficiently along z unlike the 2D configuration.

Magnetic reconnection in current sheets converts magnetic energy into particle energy, an important process in many laboratory, space, and astrophysical contexts [1]. It is the dominant mechanism by which solar wind energy enters Earth's magnetosphere [2,3]. Previous observational and theoretical studies have focused mainly on standard reconnection in large-scale current sheets, in which both ions and electrons are involved in the dynamics of this energy conversion process.

Recent observations of current sheets (CS) in Earth's highly turbulent magnetosheath region downstream of a quasiparallel bow shock revealed a new form of reconnection involving only electrons, with no ion coupling [4]. In the electron-only reconnection events, the electron-scale reconnection CS was not embedded inside of an ion-scale CS as expected for a crossing of the electron diffusion region associated with standard ion-coupled reconnection [5–7]. Having wider CS at scales comparable to the ion inertial scale is not sufficient to induce ion coupling, as observations of Earth's bow shock have found electron-only reconnection with no ion response inside ion scale CS [8,9].

Simulation have shown that ions become decoupled from reconnecting magnetic field when the length of the CS (in the outflow direction) is a few inertial lengths d_i [10] up to around ten d_i [11], depending on plasma conditions.

Since the length scale size of turbulent magnetic structures in the magnetosheath can be quite small, exhibiting correlation scales on the order of 1-10 d_i [12,13], electron-only reconnection may be the dominant form of reconnection in the turbulent magnetosheath and bow shock. Local kinetic simulations of Earth's bow shock find that electron-only reconnection is a frequent occurrence [14].

In collisionless turbulence, reconnection has been suggested to drive the energy dissipation at kinetic scales [15–17]. Below ion kinetic length scales, models suggest that the aspect ratio of turbulence eddies is governed by the balance of the eddies' turnover time with reconnection timescale mediated from electron tearing mode [18], which may facilitate a dominant form of magnetic energy release with further steepening of the energy spectrum [19]. The magnetic structures embedded in turbulence may be strongly 3D in nature, being limited in all directions. This fact and the prevalence of electron-only reconnection highlight the need for a kinetic study of 3D reconnection at electron scales.

In this study, we employ particle-in-cell (PIC) kinetic simulations of force-free CS with an out of reconnection plane (guide) magnetic field to study the 3D properties of electron reconnection. In the 3D simulation, multiple X-lines of finite extent spontaneously developed. Comparison with a

2D simulation reveals that $E_\parallel$ and hence the local reconnection rate is significantly larger in three dimensions. A control volume analysis of the 3D diffusion region shows a net mass flux in the out-of-plane direction (X-line direction) enabling a larger inflow velocity along the normal direction, leading to a faster reconnection rate.

We performed simulations in two and three dimensions using the PIC code P3D [20]. The normalizations are magnetic fields and density to B_0 and n_0, time to $\Omega_{ce}^{-1} = m_e c/eB_0$, speeds to $c_{Ae} = B_0/\sqrt{4\pi m_e n_0}$, lengths to $d_e = c_{Ae}/\Omega_{ce}$, electric fields to $E_0 = c_{Ae}B_0/c$, where c is the speed of light and temperatures to $T_0 = m_e c_{Ae}^2$. A realistic mass ratio $m_i/m_e = 1836$, 10^3 particles-per-grid (ppg), speed of light $c/c_{Ae} = 2.33$ and uniform density $n = 1$ are chosen for both simulations. The ion and electron temperatures are $T_i = 2.7$ and $T_e = 0.27$, giving the Debye length $\lambda_{De} = \sqrt{2T_e}/c \simeq 0.31$ and the electron gyroradius $\rho_e = \sqrt{2T_e} \simeq 0.73$. The 2D domain lengths $L_x \times L_y$ are $42.84d_e \times 42.84d_e$, while 3D $L_x \times L_y \times L_z$ are $42.84d_e \times 42.84d_e \times 192.77d_e$, with grid scale $\Delta \simeq 0.1674$, and time step $dt \simeq 0.06$. We use periodic boundary conditions in all directions and force-free initial conditions, with the initial magnetic fields given by $B_x = \tanh[(y - 0.25L_y)/w_0] - \tanh[(y - 0.75L_y)/w_0] - 1$ and $B_z = \sqrt{1 + B_g^2 - B_x^2}$, where $w_0 \simeq 1d_e$ is the half width of the initial CS, $B_g = 1$ is the asymptotic guide field.

The initial CS consists solely of electron current with ions as a neutralizing background where magnetic reconnection onset is from particle noise.

In three dimensions, many finite-length X-lines grow throughout the simulation domain, indicated by intense
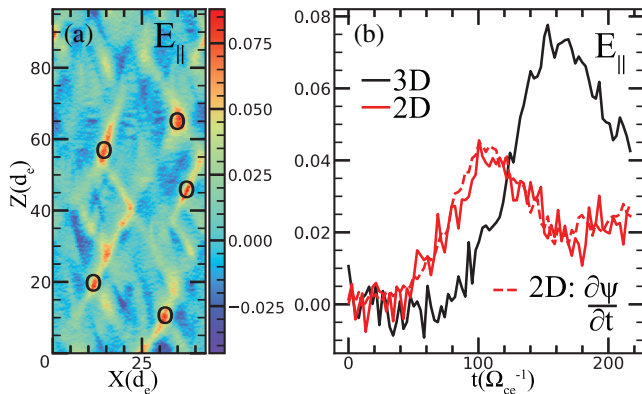

FIG. 1. (a) $E_\parallel$ over half the 3D simulation domain at $t = 152\Omega_{ce}^{-1}$ in the xz plane at $y = 32.13$. The black circles are locations of X-lines associated with intense $E_\parallel$. The time evolution of one reconnection site located at $(x, y, z) = (14.14, 32.13, 55.27)$ is examined in (b). (b) Time evolution of peak $E_\parallel$ values are shown for 2D (red) and 3D (black) simulations. The solid curves show measurements of peak $E_\parallel$ around the X-line, while the dashed red line is calculated using the magnetic vector potential ψ.

$E_\parallel$ (black circles) in Fig. 1(a) at the center of one of the CS (xz plane), while zero guide field simulation (not shown) did not produce such localized $E_\parallel$. As they form, the X-lines propagate along the equilibrium electron current ($-\hat{z}$), as seen in previous fluid 3D simulations in the ion-coupled [21,22] and electron-only [23,24] regimes. However, in ion-scale current layers, simulations revealed that the X-line spreads in the current direction [25–27].

Before onset, we measure $E_\parallel$ at the location where the X-line initially forms and after the onset, we record the peak $E_\parallel$ in the vicinity of the X-line. In three dimensions, this vicinity is the region of a finite length X-line extended in z. In two dimensions, it is a spread of few grid points from the X-line. Reconnection onset is around $t \approx 46\Omega_{ce}^{-1}$ in 2D [Fig. 1(b)] for the X-line located at $x, y = 14.14, 32.13$ [Fig. 2(a)]. In three dimensions, the same method is applied except that onset occurs at $t \approx 75\Omega_{ce}^{-1}$ [Fig. 1(b)] for the X-line located at $x, y, z = 14.14, 32.13, 55.27$ [Fig. 1(a)]. To remove fluctuations in $E_\parallel$ associated with reconfiguration of the initial CS, at each time the average of $E_\parallel$ is calculated at the center of the CS (a line in x in two dimensions and a xz plane in three dimensions) then subtracted from the peak $E_\parallel$ to give the curve (black and red) in Fig. 1(b). As a cross-check of this method, the 2D reconnection rate is calculated in the more standard way as the difference in magnetic flux between the X-line and the O-line yielding results (dashed red line) similar to the method using direct $E_\parallel$ measurements. Note, numerical modeling studies have calculated reconnection rate in stationary 3D X-line using the change of magnetic flux [28–30].

In Fig. 1(b), a striking difference between the reconnection rate $E_\parallel$ in two and three dimensions is illustrated by a fast rise in the reconnection rate with a peak rate at $\sim 100\Omega_{ce}^{-1}$ and $\sim 152\Omega_{ce}^{-1}$, respectively. In three dimensions, the peak value of $E_\parallel$ is 7.76×10^{-2}, approximately twice the 2D peak value. 3D physics enhances the reconnection rate after the reconnection onset, which is not impacted when numerical factors such as grid spacing and ppg are changed.

To determine the cause of this enhanced reconnection rate, we study the two X-lines highlighted in Fig. 1(b) at the times of peak reconnection as illustrated in Fig. 2. Compared to two dimensions in Fig. 2(a), the measured $E_\parallel$ in three dimensions at the X-line is enhanced, shown by a region of dark red around the center in Fig. 2(b). The electron inflow velocities V_{ey} are also enhanced in three dimensions [Fig. 2(d)] compared to 2D inflow velocities [Fig. 2(c)]. Figures 2(e)(2D) and (f)(3D) reveal peak values of V_{ey}, $V_{e\perp y}$ (vertical inflows perpendicular to the local magnetic fields), E_z and $E_\parallel$ in three dimensions are approximately twice as large as in two dimensions. In the same panels, the localized $E_\parallel$ structure is shown to be embedded within the CS as seen from the width associated with the reversal of the reconnecting magnetic field B_x. Both two and three dimensions show some localization of E_z but are not confined to the CS. The peak V_{ey} and $V_{e\perp y}$
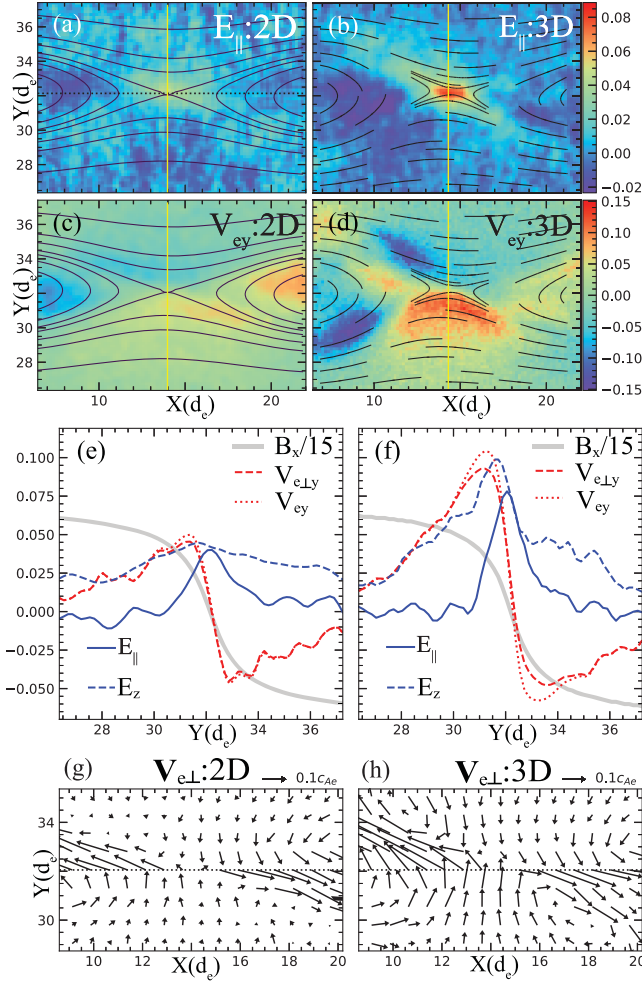
FIG. 2. 2D (left column) and 3D (right column at $z = 55.27$) results at $\sim 100\Omega_{ce}^{-1}$ and $\sim 152\Omega_{ce}^{-1}$, respectively, for the X-lines investigated in Fig. 1(b). The black contour lines in (a) and (c) are magnetic field lines while the black curves in (b) and (d) are short segments approximating projected magnetic field lines. The parallel electric field $E_{\parallel}$ is in (a) and (b). Panels (c) and (d) are inflows V_{ey}. In (e) and (f) are vertical cuts of $B_x, V_{ey}, V_{e\perp y}, E_z$, and $E_{\parallel}$ along the vertical yellow lines in panels (a)–(d). The projection of electron flows on the xy plane are the perpendicular flows $\mathbf{V}_{e\perp}$ in panel (g),(h).
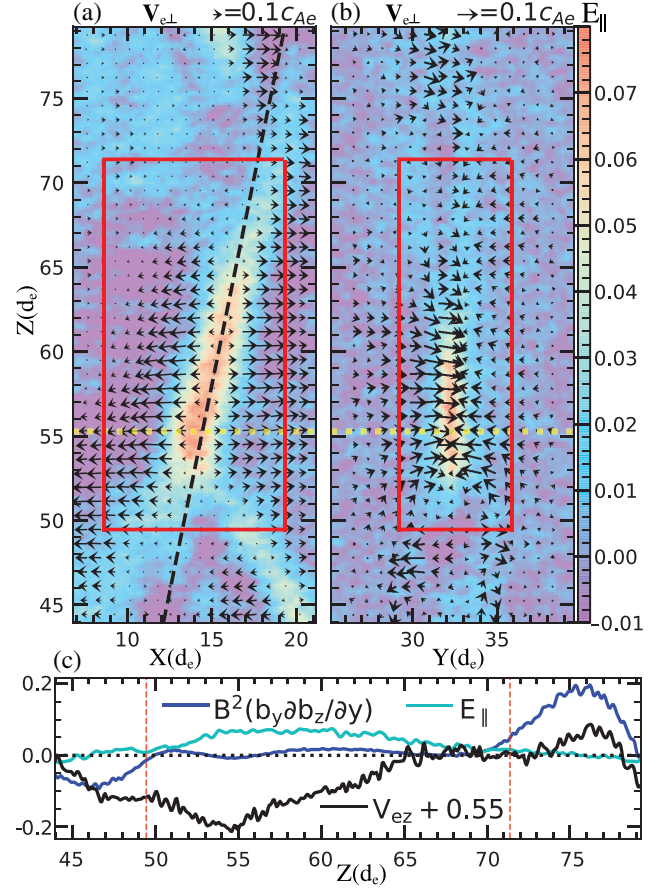

FIG. 3. (a) 3D electron flows $\mathbf{V}_{e\perp}$ at $y = 32.13$ in the xz plane are diverging from the slanted dashed black line. (b) 3D electron flows $\mathbf{V}_{e\perp}$ converge inside the red boxed boundary in the yz plane. The images of $E_{\parallel}$ in the (a) and (b) are overlaid, showing its finite and localized structure. (c) Cuts along the dashed black line in (a) are shown for V_{ez}, $E_{\parallel}$, and $B^2 b_y \partial b_z / \partial y$. The dashed vertical red lines denote z boundaries of the red boxes in (a),(b).

are almost identical in the inflow region with speeds ~ 0.1 in three dimensions [Fig. 2(f)] and ~ 0.05 in two dimensions [Fig. 2(e)]. The larger reconnection rate in three dimensions compared to two dimensions is because the inflowing velocity in three dimensions is enhanced.

The perpendicular flows $\mathbf{V}_{e\perp}$ [Figs. 2(g)(2D) and 2(h) (3D)] show a distinct inflow and outflow pattern of the electrons, indicating similar qualitative dynamics in two and three dimensions. In three dimensions, however, the velocity fields have more of a vortexlike pattern on either side of the primary perpendicular electron flows. Prominent structures are located at about (11.14,34.27) and (17.14,30.00) in Fig. 2(h). This structure extends in z,

giving an almost-spiral electron flow, that are not as outstanding in 2D [Fig. 2(g)], making 3D electron outflows more spatially localized.

Additionally, 3D reconnection is nonuniform along z as seen in the $E_{\parallel}$ structure and $\mathbf{V}_{e\perp}$ flow pattern in Fig. 3. In Fig. 3(a), the outflowing plasma $\mathbf{V}_{e\perp}$ is ejected away from the slanted black dashed line. A dotted horizontal yellow line ($z = 55.27$) is drawn at the peak value of $E_{\parallel}$. For $z < 55.27$, the exhaust forms away from the dashed line following closely with the spread of $E_{\parallel}$. Similarly, the inflowing plasma in Fig. 3(b) is nonuniform along z. The $\mathbf{V}_{e\perp}$ points in $-\hat{y}$ above $y = 32.13$ and in $+\hat{y}$ below $y = 32.13$. The extension of the X-line is about $20d_e \sim 0.5d_i$ in $\hat{z}$ shown by the length of the red boxes in Figs. 3(a), 3(b). In Fig. 3(c), cuts along the dashed black line in Fig. 3(a) reveal a net flow along z away from the peak in $E_{\parallel}$. This net flow is illustrated by the deviation of $\delta V_{ez} = V_{ez} + 0.55$ from the mean flow which is positive (negative) for z greater than (less than) the position of the peak in $E_{\parallel}$,
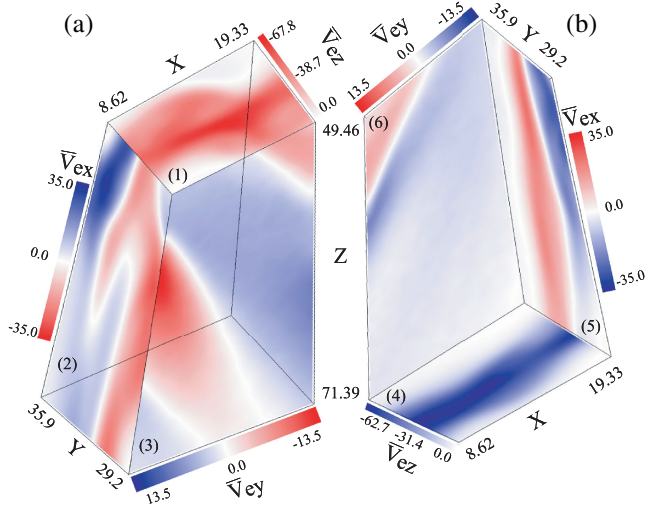
FIG. 4. 3D flow into and out of the diffusion region, where $\bar{\mathbf{V}}_e = \mathbf{V}_e \times 10^2$. Panels (a) and (b) show normal flow through each of the six faces of the diffusion region, which are numbered. For example, normal flow through face 1 at $z = 49.46$ is given by V_{ez}. The integrated mass flux [Eq. (1)] through each face is: $\Phi_{1,\ldots,6} \approx 20.6, 1.5, -2.7, -17.9, 1.22, -2.91$.

where the mean flow of -0.55 is calculated by taking the average of V_{ez} at the midplane. This outflow along z is driven by magnetic tension just as the conventional outflow in two dimensions is driven by tension. Outside the red box, the z component of magnetic tension force $B^2(\mathbf{b} \cdot \nabla)\mathbf{b}$ (blue curve) points away from the underlying $E_\parallel$ structure, where $\mathbf{b} = \mathbf{B}/|\mathbf{B}|$. To sustain the net mass flux in the z direction, the 3D diffusion region develops larger inflow velocities and thus larger $E_\parallel$.

The enhancement of $E_\parallel$ in three dimensions is linked to the increment of the speed of $V_{ey} \approx V_{e\perp y} \simeq V_{in}$ as shown in Fig. 2(f); this is because in the presence of the guide field at the X-line, $E_\parallel \simeq E_z$ and $E_z = V_{in}B_{up}/c$ since $\mathbf{E} \cdot \mathbf{B} = 0$ and $\mathbf{V}_\perp = c(\mathbf{E} \times \mathbf{B})/|\mathbf{B}|^2$ in the upstream region, where V_{in} is the upstream inflow speed and B_{up} is the upstream reconnecting magnetic field. We employ a 3D steady state control volume analysis [31] to the region of elevated $E_\parallel$ to probe how this increase of V_{in} is sustained in 3D versus 2D.

In Fig. 4, we choose a cuboid region enclosing the $E_\parallel$ structure shown by the red boxes in Figs. 3(a) and 3(b). Because there is little or no ion response, quasineutrality requires $\nabla \cdot \mathbf{V}_e \approx 0$. In discretized integral form, the mass flux through each face of the cuboid is given by

$$\Phi_j = \sum_{l,m}[\mathbf{V}_{e,j}(l,m) \cdot \hat{n}_j]\Delta^2, \qquad (1)$$

where j is one of the six faces, $\hat{n}_j$ is the normal unit vector pointing out of the face, (l, m) indexes are the grid point locations on the surface of the face and Δ is the grid spacing. The calculated values for Φ_j are given in the caption of Fig. 4. The normal inflows into the diffusion box

are shown in blue. For example, V_{ey} at $y = 35.9$ in face 6 mostly consists of a slanted blue strip. Similarly, the normal outflows are shown in red.

From Eq. (1), the net mass flux in z is $\Phi_1 + \Phi_4 \approx 2.72$. In y, the sum of mass fluxes is $\Phi_3 + \Phi_6 \approx -5.61$. Finally, the sum of mass fluxes in x is $\Phi_2 + \Phi_5 \approx 2.72$. Thus, the net outward mass flux from the diffusion region along z is comparable to the sum of mass fluxes in x. The total mass flux (≈ 0.17) from Eq. (1) is approximately an order of magnitude smaller than any direction's total mass flux contribution in Fig. 4, suggesting that the quasisteady approximation is reasonable.

This implies that the modification to mass continuity in three dimensions induces the net outflow along z combined with the usual outflow in x to increase the inflow along y. This is consistent with the inflowing plasma flow V_{ey} being twice as fast as that measured in two dimensions. Such asymmetry was noted in an ion-coupled reconnection laboratory experiment [32] caused by an equilibrium nonuniformity. However, we find that the asymmetry develops spontaneously from the initially uniform 1D equilibrium.

Our results demonstrate a new form of electron-only reconnection in a 3D system in which the magnetic X-line is localized in the out-of-plane (z) direction. Using PIC simulations, we explored electron-only reconnection soon after its onset, comparing one finite length X-line in three dimensions with results from two dimensions. In both two and three dimensions, the parallel electric field is largest in the vicinity of the X-line and is equivalent to the local reconnection rate E_z. While both E_z and $E_\parallel$ are spatially localized near the X-line, $E_\parallel$ is more limited in extent than E_z. The 3D simulation exhibits both a larger $E_\parallel$ and inflow velocity; roughly twice their 2D counterparts. The driver of the larger inflow velocity in three dimensions is linked with the tension force in z, which ultimately drives a net outflow along z from the diffusion region. A control volume analysis of the diffusion region covering the $E_\parallel$ structure reveals that the net mass flux along z is equal to the total mass flux along x. This increased outward mass flux allows an inflow velocity twice what is present in two dimensions, leading to twice the reconnection rate.

We now compare the large electric fields in the 3D simulation with observations. In the turbulent magneto-sheath, MMS observed large and coherent $E_\parallel$ of $\sim$7 mV/m in a reconnecting CS [4]. In the context of electron-only reconnection, a comparison between this measured $E_\parallel$ and the simulation value can be made by normalizing it to inflowing plasma parameters given by $cE_\parallel/(c_{Ae,up}B_{up})$, where $c_{Ae,up}$ is the upstream electron Alfvén speed (using B_{up}). Normalized this way with $B_{up} = 5$ nT and $n = 20$ cm^{-3}, the Phan *et al.* [4] event gives $E_\parallel \sim 1$, which is an order of magnitude larger than $E_\parallel \sim 0.08$ in 3D simulation. An upper limit on the rate of reconnection is yet to be established in the new 3D reconnection geometry as

reconnection in narrower current layers may be more localized (few d_e's) in z than in the present 3D simulation. Additionally, the guide field of the Phan *et al.* [4] event was 8 times larger than the guide field in our simulation, which could account for a much larger $E_\parallel$. Lastly, it is possible that reconnection embedded in fully developed turbulence [33–35] could produce conditions leading to an enhanced $E_\parallel$.

The spatial structure of the electric fields measured by MMS have significant differences from simulations, although both demonstrated highly spatially localized $E_\parallel$. The 2D and 3D simulations reconnected robustly for a duration $\sim 100\Omega_{ce}^{-1}$ [Fig. 1(b)] and both exhibit some localization of E_z in the inflow direction [Figs. 2(e) and 2(f)], however, not confined within the CS. Conversely, the Phan *et al.* [4] event exhibited a highly localized E_M (simulation E_z) along the normal direction (simulation $\hat{y}$), confined within the reconnection CS. Noting that the Phan *et al.* [4] event had a guide field eight times the reconnection field and given that such a large guide field may allow the reconnection structure to be confined to a much smaller spatial region, 3D simulations with such a large guide field may exhibit such localized E_M structure. Simulating such a large guide field, especially with high plasma β, poses significant challenges for simulation because they require small time steps associated with high temperatures and long simulation domains along z.

Numerous numerical simulation studies have explored the interplay between reconnection and turbulence (e.g., Refs. [36–39]). In the MHD limit, magnetic field stochasticity in the form of 3D magnetic field wandering was shown to be essential for fast reconnection in turbulent fluid [33,40,41] and since this study has not been designed to study electron-only reconnection in self-consistently produced turbulence, the effects of stochasticity [28,35,42] is an important aspect that entails future examinations. Electron-only reconnection may play a key role in the dissipation of turbulent energy, but precisely how remains an active area of research. Since electron-only reconnection's prevalence has been observed at different regions [8,9,13,43], investigating its basic properties at kinetic scales is relevant in understanding the interplay between reconnection and turbulence. The findings presented in this Letter demonstrate that 3D reconnection at electron scales is fundamentally different than the often studied 2D reconnection paradigm and indicate that 3D effects may alter energy dissipation channels at kinetic scales. Thus, extrapolations from 2D models to explore reconnection driven energy release in real systems must be taken with caution. How localized electron scale reconnection effects and controls large scale reconnection physics will require future investigations.

---

[*] pspyakurel@berkeley.edu

[1] M. Yamada, R. Kulsrud, and H. Ji, Rev. Mod. Phys. **82**, 603 (2010).

[2] T. Nagai, M. Fujimoto, Y. Saito, S. Machida, T. Terasawa, R. Nakamura, T. Yamamoto, T. Mukai, A. Nishida, and S. Kokubun, J. Geophys. Res. **103**, 4419 (1998).

[3] V. Angelopoulos, J. P. McFadden, D. Larson, C. W. Carlson, S. B. Mende, H. Frey, T. Phan, D. G. Sibeck, K. Glassmeier, U. Auster, E. Donovan, I. R. Mann, I. J. Rae, C. T. Russell, A. Runov, X. Zhou, and L. Kepko, Science **321**, 931 (2008).

[4] T. D. Phan *et al.*, Nature (London) **557**, 202 (2018).

[5] J. L. Burch *et al.*, Science **352**, aaf2939 (2016).

[6] F. D. Wilder, R. E. Ergun, S. Eriksson, T. D. Phan, J. L. Burch, N. Ahmadi, K. A. Goodrich, D. L. Newman, K. J. Trattner, R. B. Torbert, B. L. Giles, R. J. Strangeway, W. Magnes, P.-A. Lindqvist, and Y.-V. Khotyaintsev, Phys. Rev. Lett. **118**, 265101 (2017).

[7] S. Eriksson, F. D. Wilder, R. E. Ergun, S. J. Schwartz, P. A. Cassak, J. L. Burch, L.-J. Chen, R. B. Torbert, T. D. Phan, B. Lavraud *et al.*, Phys. Rev. Lett. **117**, 015001 (2016).

[8] I. Gingell, S. J. Schwartz, J. P. Eastwood, J. L. Burch, R. E. Ergun, S. Fuselier, D. J. Gershman, B. L. Giles, Y. V. Khotyaintsev, B. Lavraud, P.-A. Lindqvist, W. R. Paterson, T. D. Phan, C. T. Russell, J. E. Stawarz, R. J. Strangeway, R. B. Torbert, and F. Wilder, Geophys. Res. Lett. **46**, 1177 (2019).

[9] S. Wang, L.-J. Chen, N. Bessho, M. Hesse, L. B. Wilson III, B. Giles, T. E. Moore, C. T. Russell, R. B. Torbert, and J. L. Burch, Geophys. Res. Lett. **46**, 562 (2019).

[10] M. E. Mandt, R. E. Denton, and J. F. Drake, Geophys. Res. Lett. **21**, 73 (1994).

[11] P. Sharma Pyakurel, M. A. Shay, T. D. Phan, W. H. Matthaeus, J. F. Drake, J. M. TenBarge, C. C. Haggerty, K. G. Klein, P. A. Cassak, T. N. Parashar, M. Swisdak, and A. Chasapis, Phys. Plasmas **26**, 082307 (2019).

[12] J.-S. He, E. Marsch, C.-Y. Tu, Q.-G. Zong, S. Yao, and H. Tian, J. Geophys. Res. **116**, A06207 (2011).

[13] J. E. Stawarz, J. P. Eastwood, T. D. Phan, I. L. Gingell, M. A. Shay, J. L. Burch, R. E. Ergun, B. L. Giles, D. J. Gershman, O. L. Contel, P.-A. Lindqvist, C. T. Russell, R. J. Strangeway, R. B. Torbert, M. R. Argall, D. Fischer, W. Magnes, and L. Franci, Astrophys. J. **877**, L37 (2019).

[14] N. Bessho, L.-J. Chen, S. Wang, M. Hesse, and L. B. Wilson III, Geophys. Res. Lett. **46**, 9352 (2019).

[15] W. H. Matthaeus and S. L. Lamkin, Phys. Fluids **29**, 2513 (1986).

[16] A. Retinò, D. Sundkvist, A. Vaivads, F. Mozer, M. André, and C. J. Owen, Nat. Phys. **3,** 235 (2007).

[17] S. Servidio, W. H. Matthaeus, M. A. Shay, P. A. Cassak, and P. Dmitruk, Phys. Rev. Lett. **102,** 115003 (2009).

[18] S. Boldyrev and N. F. Loureiro, Phys. Rev. Research **1,** 012006(R) (2019).

[19] N. F. Loureiro and S. Boldyrev, Astrophys. J. **890,** 55 (2020).

[20] A. Zeiler, D. Biskamp, J. F. Drake, B. N. Rogers, M. A. Shay, and M. Scholer, J. Geophys. Res. **107,** 1230 (2002).

[21] J. D. Huba and L. I. Rudakov, Phys. Plasmas **9,** 4435 (2002).

[22] M. A. Shay, J. F. Drake, M. Swisdak, W. Dorland, and B. N. Rogers, Geophys. Res. Lett. **30,** 1345 (2003).

[23] N. Jain, A. S. Sharma, L. M. Zelenyi, and H. V. Malova, Ann. Geophys. **30,** 661 (2012).

[24] N. Jain, J. Büchner, S. Dorfman, H. Ji, and A. Surjalal Sharma, Phys. Plasmas **20,** 112101 (2013).

[25] T. K. M. Nakamura, R. Nakamura, A. Alexandrova, Y. Kubota, and T. Nagai, J. Geophys. Res. **117** (2012).

[26] L. S. Shepherd and P. A. Cassak, J. Geophys. Res. **117** (2012).

[27] T. C. Li, Y.-H. Liu, M. Hesse, and Y. Zou, J. Geophys. Res. **125,** e2019JA027094 (2020).

[28] G. Kowal, A. Lazarian, E. T. Vishniac, and K. Otmianowska-Mazur, Astrophys. J. **700,** 63 (2009).

[29] Y.-H. Liu, T. C. Li, M. Hesse, W. J. Sun, J. Liu, J. Burch, J. A. Slavin, and K. Huang, J. Geophys. Res. **124,** 2819 (2019).

[30] K. Huang, Y.-H. Liu, Q. Lu, and M. Hesse, Geophys. Res. Lett. **47,** e2020GL088147 (2020).

[31] J. C. Meyer, Structure of the diffusion region in three dimensional magnetic reconnection, Ph.D. thesis, University of Delaware, 2015.

[32] S. Dorfman, H. Ji, M. Yamada, J. Yoo, E. Lawrence, C. Myers, and T. D. Tharp, Geophys. Res. Lett. **40,** 233 (2013).

[33] A. Lazarian and E. Vishniac, Astrophys. J. **517,** 700 (1999).

[34] A. Lazarian, G. Kowal, E. Vishniac, K. Kulpa-Dubel, and K. Otmianowska-Mazur, Highlights Astronomy **5,** 434 (2010).

[35] A. Lazarian, G. L. Eyink, A. Jafari, G. Kowal, H. Li, S. Xu, and E. T. Vishniac, Phys. Plasmas **27,** 012305 (2020).

[36] S. S. Cerri and F. Califano, New J. Phys. **19,** 025007 (2017).

[37] A. Mallet, A. A. Schekochihin, and B. D. G. Chandran, Mon. Not. R. Astron. Soc. **468,** 4862 (2017).

[38] F. Califano, S. S. Cerri, M. Faganello, D. Laveder, and M. W. Kunz, Front. Phys. **8,** 317 (2020).

[39] S. Adhikari, M. A. Shay, T. N. Parashar, P. S. Pyakurel, W. H. Matthaeus, D. Godzieba, J. E. Stawarz, J. P. Eastwood, and J. T. Dahlin, Phys. Plasmas **27,** 042305 (2020).

[40] G. L. Eyink, A. Lazarian, and E. T. Vishniac, Astrophys. J. **743,** 51 (2011).

[41] G. Eyink, E. Vishniac, C. Lalescu, H. Aluie, K. Kanov, K. Bürger, R. Burns, C. Meneveau, and A. Szalay, Nature (London) **497,** 466 (2013).

[42] G. Kowal, D. A. Falceta-Gonçalves, A. Lazarian, and E. T. Vishniac, Astrophys. J. **892,** 50 (2020).

[43] M. Hubbert, Y. Qi, C. T. Russell, J. L. Burch, B. L. Giles, and T. E. Moore, Geophys. Res. Lett. **48,** e2020GL091364 (2021).

[44] Computational and Information Systems Laboratory, Cheyenne: HPE/SGI ICE XA System (University Community Computing), (2017).